Staufen2 functions in Staufen1-mediated mRNA decay by binding to itself and its paralog and promoting UPF1 helicase but not ATPase activity

Eonyoung Park[a,b], Michael L. Gleghorn[a,b], and Lynne E. Maquat[a,b,1]

[a]Department of Biochemistry and Biophysics, School of Medicine and Dentistry, and [b]Center for RNA Biology, University of Rochester, Rochester, NY 14642

This contribution is part of the special series of Inaugural Articles by members of the National Academy of Sciences elected in 2011.

Edited by Michael R. Botchan, University of California, Berkeley, CA, and approved November 16, 2012 (received for review August 3, 2012)

Staufen (STAU)1-mediated mRNA decay (SMD) is a posttranscriptional regulatory mechanism in mammals that degrades mRNAs harboring a STAU1-binding site (SBS) in their 3′-untranslated regions (3′ UTRs). We show that SMD involves not only STAU1 but also its paralog STAU2. STAU2, like STAU1, is a double-stranded RNA-binding protein that interacts directly with the ATP-dependent RNA helicase up-frameshift 1 (UPF1) to reduce the half-life of SMD targets that form an SBS by either intramolecular or intermolecular base-pairing. Compared with STAU1, STAU2 binds ∼10-fold more UPF1 and ∼two- to fivefold more of those SBS-containing mRNAs that were tested, and it comparably promotes UPF1 helicase activity, which is critical for SMD. STAU1- or STAU2-mediated augmentation of UPF1 helicase activity is not accompanied by enhanced ATP hydrolysis but does depend on ATP binding and a basal level of UPF1 ATPase activity. Studies of STAU2 demonstrate it changes the conformation of RNA-bound UPF1. These findings, and evidence for STAU1–STAU1, STAU2–STAU2, and STAU1–STAU2 formation in vitro and in cells, are consistent with results from tethering assays: the decrease in mRNA abundance brought about by tethering siRNA-resistant STAU2 or STAU1 to an mRNA 3′ UTR is inhibited by downregulating the abundance of cellular STAU2, STAU1, or UPF1. It follows that the efficiency of SMD in different cell types reflects the cumulative abundance of STAU1 and STAU2. We propose that STAU paralogs contribute to SMD by "greasing the wheels" of RNA-bound UPF1 so as to enhance its unwinding capacity per molecule of ATP hydrolyzed.

protein–protein interactions | protein-RNA interactions

Mammalian cells contain two Staufen (STAU) paralogs, STAU1 and STAU2. Each derives from a separate gene that produces multiple protein isoforms via alternative pre-mRNA splicing and/or polyadenylation. Every STAU1 and STAU2 isoform contains multiple conserved dsRNA-binding domains (RBDs), of which dsRBD3 and dsRBD4 constitute the major if not sole active dsRNA-binding sites (1, 2).

Although STAU1 and probably STAU2 are expressed ubiquitously, STAU2 is most abundant in heart and brain (1, 3). Both paralogs are present in ribonucleoprotein particles (RNPs) within neuronal cell bodies and dendrites (1, 4–7). Both are also involved in the microtubule-dependent transport of RNAs to dendrites of polarized neurons (5, 8), presumably via the tubulin-binding domain (2). Moreover, both paralogs play a crucial role in the formation and maintenance of the dendritic spines of hippocampal neurons and are required for synaptic plasticity and memory (7, 9–11), although the detection of paralog-specific RNA granules in the distal dendrites of rat hippocampal neurons has been used to argue for paralog-distinct functions (1). Additional support for paralog-specific roles derives from the demonstration using rat hippocampal slice cultures that STAU1 but not STAU2 functions in the late phase of forskolin-induced long-term potentiation (10–12), whereas STAU2 but not STAU1 is involved in metabotropic glutamate receptor-mediated long-term depression (12). As another example of apparent paralog specificity, we have shown that STAU1 degrades mRNAs that harbor a STAU1-binding site (SBS) downstream of their normal termination codon in a pathway called STAU1-mediated mRNA decay or SMD (13, 14), and work published by others indicates that SMD does not involve STAU2 (3, 15).

According to our current model for SMD, when translation terminates upstream of an SBS, recruitment of the nonsense-mediated mRNA decay (NMD) factor UPF1 to SBS-bound STAU1 triggers mRNA decay. SMD influences a number of cellular processes, including the differentiation of mouse C2C12 myoblasts to myotubes (16), the motility of human HaCaT keratinocytes (17), and the differentiation of mouse 3T3-L1 preadipocytes to adipocytes (18). Thus, SMD may explain the essential role of STAU1 in embryonic stem-cell differentiation (19).

We report here that SMD is triggered not only by STAU1 but also by STAU2, each of which can self-associate as well as associate with one another. Our findings that SMD requires the ATP-dependent helicase activity of UPF1, each STAU paralog promotes UPF1 helicase activity without promoting UPF1 ATP hydrolytic activity, and STAU2 increases the RNA footprint of UPF1 allow us to expand on the existing model for SMD. We propose that STAU paralog-binding to UPF1 induces a change in UPF1 conformation that resembles its conformation during intermediate or product steps of ATP hydrolysis and enhances the amount of unwinding per ATP molecule hydrolyzed.

Results

STAU2 Functions in SMD. Human embryonic kidney (HEK) 293T and HeLa cells express multiple isoforms of STAU2 and STAU1 (1, 13, 20) (Fig. 1*A* and Fig. S1*A*). STAU2 and STAU1 are ∼50% identical (20). dsRBDs 3 and 4 have retained the ability to bind dsRNA and are 78% and 81% identical, respectively (2). dsRBD2, which is 48% identical between the two paralogs, and dsRBD5, the full-length of which is unique to STAU1 (21) (Fig. 1*A*), have been implicated in the formation of STAU1 homodimers and homomultimers in complex with RNA (22).

To assay for STAU2 function in SMD, STAU2 and, for comparison, STAU1 were down-regulated to the same extent in HeLa cells, where their abundance is comparable (Fig. S1 *B* and *C*). Subsequently, the levels of SMD reporters (normalized to the level of a reference mRNA to control for variations in cell transfection) and a cellular SMD target (normalized to the level of its pre-mRNA to control for effects on transcription) were quantitated. Thus, HeLa cells were transiently transfected with the phCMV-MUP [which produces major urinary protein (MUP) mRNA driven by a cytomegalovirus (CMV) promoter] reference plasmid

Author contributions: E.P., M.L.G., and L.E.M. designed research; E.P. and M.L.G. performed research; E.P., M.L.G., and L.E.M. analyzed data; and E.P., M.L.G., and L.E.M. wrote the paper.

The authors declare no conflict of interest.

This article is a PNAS Direct Submission.

[1]To whom correspondence should be addressed. E-mail: lynne_maquat@urmc.rochester.edu.

This article contains supporting information online at www.pnas.org/lookup/suppl/doi:10.1073/pnas.1213508110/-/DCSupplemental.

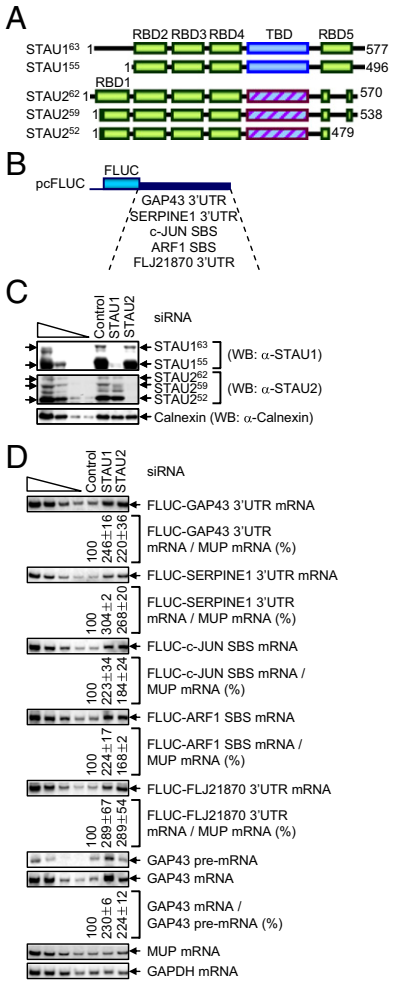

Fig. 1. siRNA-mediated down-regulation of STAU2 inhibits SMD. (*A*) Diagrams of human STAU1 and STAU2 isoforms, where boxes represent functional and/or structural domains. 1, N-terminal amino acid; TBD, tubulin-binding domain (where the hatched STAU2 TBD is ~18% identical to the STAU1 TBD). (*B*) Partial diagrams of pcFLUC SMD-reporter plasmids. (*C* and *D*) HeLa cells (4×10^6 per 100-mm dish) were transiently transfected with 1.5 μg of each pcFLUC SMD-reporter plasmid and 1 μg of the phCMV-MUP reference plasmid. Cells were retransfected 1 d later with 100 nM of Control siRNA, STAU1 siRNA, or STAU2 siRNA and harvested 2 d later. (*C*) WB, where Calnexin controlled for variations in protein loading. The left-most four lanes show serial threefold dilutions of protein. Arrows pointing right denote STAU isoforms, and unidentified bands do not interfere with the analyses. (*D*) RT-PCR, where the level of each FLUC mRNA was normalized to the level of MUP mRNA, the level of cellular GAP43 mRNA was normalized to the level of its pre-mRNA, and normalized levels in the presence of Control siRNA were defined as 100. All results are representative of at least three independently performed experiments.

and a mixture of the five pcFLUC SMD-reporter plasmids, which encode firefly luciferase (FLUC) mRNAs and vary in their 3′ UTRs (Fig. 1*B*) (13, 14, 17). The 3′ UTRs consist of the growth-associated protein 43 (GAP43) 3′ UTR, the serpin peptidase inhibitor, clade E (nexin, plasminogen activator inhibitor type 1), member 1 (SERPINE1) 3′ UTR, the v-jun avian sarcoma virus 17 oncogene homolog (c-JUN) SBS (nucleotides 485–675 of the c-JUN 3′ UTR), the ADP-ribosylation factor 1 (ARF1) SBS (nucleotides 1–300 of the ARF1 3′UTR), or the ankyrin-repeat domain 57 (FLJ21870, also called ANKRD57) 3′ UTR. The ARF1 SBS and probably the GAP43 and c-JUN SBSs are formed by intramolecular base-pairing, whereas the SERPINE1 and FLJ21870 SBSs are formed by intermolecular base-pairing with a long-noncoding RNA (1/2-sbsRNA1) via partially complementary Alu elements (17). One day later, cells were transiently transfected with Control, STAU1, or STAU2 siRNA.

Western blotting (WB) demonstrated that STAU1 and STAU2 siRNAs specifically reduced the levels of their target isoforms to <10% the levels in Control siRNA-treated cells (Fig. 1*C*). RT-PCR revealed that STAU1 and STAU2 siRNAs augmented the level of each SMD reporter mRNA ~two- to threefold, indicating that each paralog functions in SMD to a comparable extent [Fig. 1*D*; corroborating RT–quantitative PCR (qPCR) data in Fig. S1*D* and data obtained using STAU2(A) or STAU2(B) siRNA in Fig. S1 *E* and *F*]. Consistent with STAU2 function in SMD, STAU2 siRNA, like STAU1 siRNA, up-regulated the level of endogenous GAP43 mRNA (Fig. 1*D* and Fig. S1*F*) and reduced the half-life of mRNA harboring a 3′ UTR SBS (Fig. S1 *G–I*).

STAU2, Like STAU1, Interacts Directly with UPF1. To begin to assess STAU2 isoforms for function in SMD, extracts of HeLa cells that stably express FLAG-UPF1 at ≤twofold the level of cellular UPF1 (23) were immunoprecipitated in the presence or absence of RNase A using anti-FLAG or, as a control for nonspecific immunoprecipitation (IP), mouse (m)IgG. Approximately 10% of each isoform of STAU1 or STAU2 coimmunoprecipitated with FLAG-UPF1 (Fig. 2*A*). Furthermore, compared with the STAU1 isoforms (see also ref. 18), the co-IP efficiency of each

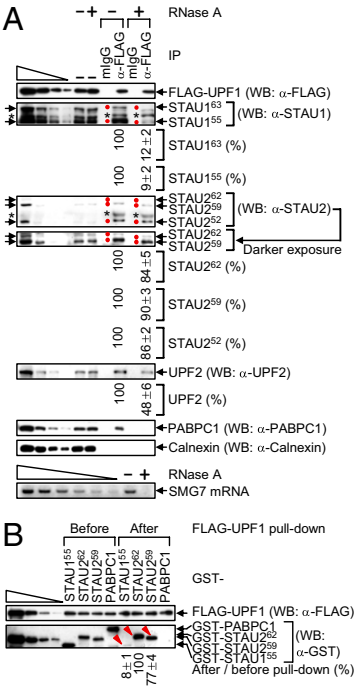

Fig. 2. Compared with STAU1 isoforms, STAU2 isoforms interact more efficiently with UPF1. (*A*) HeLa cells stably expressing FLAG-UPF1 (8×10^7 per 150-mm dish) were lysed and analyzed before (–) or after IP using anti(α)-FLAG or, as a negative control, mouse (m)IgG in the absence (–) or presence (+) of RNase A. WB was performed, where the left-most four lanes show threefold dilutions of protein before IP. Arrows pointing right and red dots denote STAU isoforms, and the asterisks specify unidentified proteins. The level of each coimmunoprecipitated STAU protein in the absence of RNase A was defined as 100. (*A, Lower*) SMG7 mRNA was analyzed using RT-PCR before IP to demonstrate that the RNase A digestion was complete. The left-most six lanes represent twofold dilutions of RNA. (*B*) GST-STAU1^{55}, GST-STAU2^{62}, GST-STAU2^{59}, or GST-PABPC1 purified from *E. coli* (100 nM) was incubated with baculovirus-produced and purified FLAG-UPF1 (200 nM), subjected to FLAG-UPF1 pull-down, and analyzed using WB. Protein levels after pull-down were normalized to the level before pull-down, and the normalized level of GST-STAU2^{62} was defined as 100. The left-most four lanes show threefold dilutions of protein. Red arrowheads denote the GST-STAU protein under analysis (Fig. S2*B*).

STAU2 isoform was ~10-fold more resistant to RNase A (Fig. 2*A*). As indications that RNase A treatment was successful, the co-IP of UPF2 with FLAG-UPF1 was partially sensitive to RNase A (Fig. 2*A*) (24), the co-IP of poly(A)-binding protein C1 (PABPC1) was completely sensitive to RNase A (Fig. 2*A*) (24), and cellular suppressor with morphogenetic effect on genitalia protein 7 (SMG7) mRNA was detectable in the absence but not the presence of RNase A (Fig. 2*A*). IPs of cellular UPF1 using lysates from formaldehyde cross-linked human neuroblastoma SK-N-MC cells demonstrated that STAU1 and STAU2 isoforms also coimmunoprecipitate with cellular UPF1, indicating that the interactions occur within cells rather than as an artifact after cell lysis (Fig. S2*A*).

To examine whether the interaction of STAU2 with UPF1 is direct, and to determine whether the higher association of UPF1 with STAU2 relative to STAU1 is recapitulated in vitro, GST-STAU1^{55} (13), GST-STAU2^{62}, GST-STAU2^{59} or, as a negative control, GST-PABPC1 was produced and purified from *Escherichia coli*, mixed with baculovirus-produced and purified FLAG-UPF1 (25), and subjected to FLAG-UPF1 pull-down. Of the STAU2 isoforms, we focused on STAU2^{62} and STAU2^{59} because their binding to mRNA has been characterized using a genome-wide approach (20). FLAG-UPF1 pulled down ~10-fold more GST-STAU2^{62} and GST-STAU2^{59} compared with GST-STAU1^{55} (Fig. 2*B* and Fig. S2*B*). As expected, FLAG-UPF1 failed to pull down GST-PABPC1 (Fig. 2*B*). These results are consistent with the finding that the co-IP of STAU2 with FLAG-UPF1 is less sensitive to RNase A than the co-IP of STAU1 with FLAG-UPF1.

STAU2 and STAU1 Paralogs Self-Associate and Associate with One Another. STAU1 has been found to dimerize if not multimerize with itself in vitro and in cells (22). To better define STAU2 interactions in vitro, pull-downs using *E. coli*-produced proteins (Fig. S2*C*) were performed. GST-STAU1^{55} pulled down not only HIS-STAU1^{55} but also STAU2^{62}-HIS and STAU2^{59}-HIS with comparable efficiencies and, as expected, did not pull down BSA (Fig. 3*A*). Furthermore, STAU2^{62}-HIS and STAU2^{59}-HIS pulled down a comparable amount of GST-STAU1^{55}, STAU2^{62}-GST, or STAU2^{59}-GST and, as expected, did not pull down GST-PABPC1 (Fig. 3 *B* and *C*) (26). These findings indicate that the efficiencies with which each STAU2 isoform interacts with itself, with one another, or with STAU1^{55} are indistinguishable in vitro (Fig. S2*D*).

To assay for STAU1 and STAU2 interactions in vivo, HEK293T cells were transiently transfected with a STAU1^{55}-HA$_3$ expression vector (13, 14; where it was called pSTAU1-HA) to test for the ability of STAU1^{55}-HA$_3$ to interact with cellular STAU1 and STAU2. STAU1^{55}-HA$_3$ indeed coimmunoprecipitated with cellular STAU1^{55}, STAU2^{62}, STAU2^{59}, and STAU2^{52} in the absence or presence of RNase A (Fig. 3*D*; it was not possible to assay cellular STAU1^{63} because it comigrates with STAU1^{55}-HA$_3$). Control experiments demonstrated that none of the STAU isoforms was immunoprecipitated using rat (r)IgG, Calnexin failed to coimmunoprecipitate under any circumstance, and cellular GAPDH mRNA was detectable in the absence but not the presence of RNase A (Fig. 3*D*). In related experiments, HEK293T cells were transiently transfected with a STAU2^{62}-HA$_3$ expression vector. STAU2^{62}-HA$_3$ also coimmunoprecipitated with cellular STAU2^{59} and STAU2^{52} in the absence or presence of RNase A (Fig. 3*E*; it was not possible to assay cellular STAU2^{62} because it comigrates with STAU2^{62}-HA$_3$). Control experiments showed that none of the STAU isoforms was immunoprecipitated in mock transfections involving an HA$_3$ expression vector, PLCγ1 failed to coimmunoprecipitate under any circumstance, and cellular GAPDH mRNA was detectable in the absence but not the presence of RNase A (Fig. 3*E*).

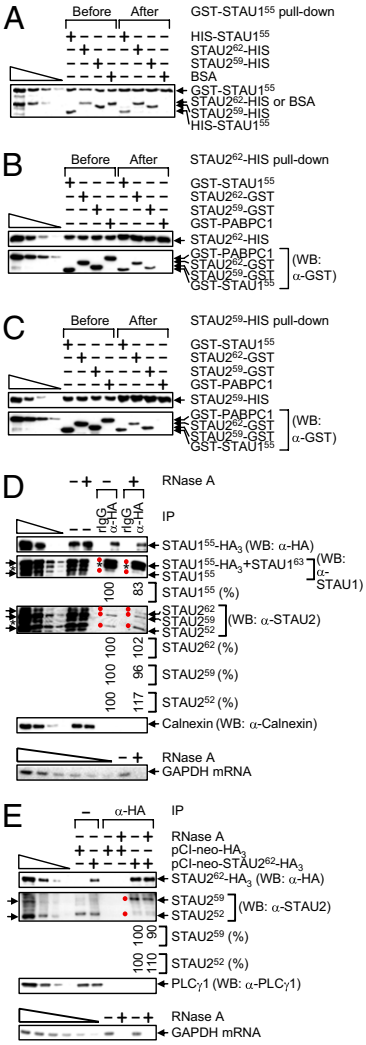

Fig. 3. STAU2^{62} and STAU2^{59} self-associate and associate with one another and with STAU1^{55}. (*A*) GST-STAU1^{55} (100 nM) was incubated with 100 nM of HIS-STAU1^{55}, STAU2^{62}-HIS, STAU2^{59}-HIS or, as a negative control, BSA, subjected to GST-STAU1^{55} pull-down, resolved in SDS-polyacrylamide, and stained using SYPRO Ruby. The left-most four lanes are threefold dilutions of GST-STAU1^{55} and BSA. (*B* and *C*) WB before and after HIS pull-down of 100 nM of STAU2^{62}-HIS (*B*) or STAU2^{59}-HIS (*C*) that was incubated with 100 nM of GST-STAU1^{55}, STAU2^{62}-GST, STAU2^{59}-GST or, as a negative control, GST-PABPC1. (*D*) HEK293T cells (4×10^7 per 150-mm dish) were transiently transfected with 10 μg of pSTAU1^{55}-HA$_3$, lysed, and analyzed before (–) or after IP using anti(α)-HA or, as a negative control, rat (r)IgG in the absence (–) or presence (+) of RNase A. The level of each coimmunoprecipitated STAU protein in the absence of RNase A was defined as 100. Arrows pointing left and red dots denote STAU isoforms, and the asterisks specify unidentified proteins. Calnexin controlled for variations in protein loading before IP and demonstrates the specificity of the IP. (*D, Lower*) GAPDH mRNA was analyzed using RT-PCR before IP to demonstrate that the RNase A digestion was complete. The six left-most lanes represent twofold serial dilutions of RNA. (*E*) HEK293T cells (4×10^7 per 150-mm dish) were transiently transfected with 5 μg of pCI-neo-HA$_3$ or pCI-neo-STAU2^{62}-HA$_3$, lysed, and analyzed before or after IP using α-HA in the absence or presence of RNase A. The level of each coimmunoprecipitated STAU1 isoform in the absence of RNase A was defined as 100. Notations, serial dilutions, and GAPDH mRNA analyses were as in *D*.

STAU2, Like STAU1, Coimmunoprecipitates with SBSs. STAU1 and STAU2 have been reported to bind distinct but overlapping subsets of mRNAs in HEK293T cells (20). Considering our findings that STAU2 and STAU1 interact directly (Fig. 3) and all STAU2 isoforms associate with polysomes (Fig. S2*E*), we next determined whether STAU2 coimmunoprecipitates with RNA sequences that are known to bind STAU1 and trigger SMD (13, 14, 16).

HeLa cells were transiently transfected with a pCI-neo-STAU1^{55}-HA$_3$, pCI-neo-STAU2^{62}-HA$_3$, or pCI-neo-STAU2^{59}-

HA_3 effector plasmid together with four of the pcFLUC SMD-reporter plasmids (Fig. 1*B*). Binding studies were performed using HeLa cells because, as noted above, they contain comparable amounts of endogenous STAU1 and STAU2 paralogs (Fig. S1 *B* and *C*), and comparable levels of $STAU1^{55}$-HA_3, $STAU2^{62}$-HA_3, and $STAU2^{59}$-HA_3 can be expressed. The pcFLUC SMD-reporter plasmids served as positive controls for $STAU1^{55}$ binding. Two days after transfection, cells were exposed to formaldehyde, and lysates were immunoprecipitated using anti-HA.

$STAU1^{55}$-HA_3, $STAU2^{62}$-HA_3, and $STAU2^{59}$-HA_3 were expressed at comparable levels before IP and immunoprecipitated with comparable efficiencies (Fig. 4*A*). $STAU2^{62}$-HA_3 and $STAU2^{59}$-HA_3 coimmunoprecipitate with FLUC SMD-reporter mRNAs ~two- to fivefold more efficiently than does $STAU1^{55}$-HA_3 (Fig. 4 *B* and *C*). Because the efficiency of paralog self-association and association with one another is comparable, and the co-IP of $STAU1^{55}$-HA_3 with the reporter mRNAs reflects binding to the SBSs, we conclude that $STAU2^{62}$ and $STAU2^{59}$ may bind other if not all SBSs more efficiently than does $STAU1^{55}$.

Tethering siRNA-Resistant STAU2 or STAU1 Downstream of a Termination Codon Reduces mRNA Abundance in a Way That Is Inhibited When Cellular STAU1, STAU2, or UPF1 Is Down-Regulated. Tethering human STAU1 sufficiently downstream of the termination codon of a reporter mRNA triggers SMD of that mRNA depending on UPF1 and translation (13, 25). Given our findings that down-regulating either STAU1 or STAU2 inhibits SMD (Fig. 1 and Fig. S1), and $STAU2^{62}$ and $STAU2^{59}$ bind UPF1, STAU1, and SBSs (Figs. 2–4), tethering STAU2 isoforms should also trigger SMD in a pathway that involves cellular UPF1 and both cellular STAU paralogs. To test this hypothesis because the literature indicates otherwise (3, 15), HeLa cells were transiently

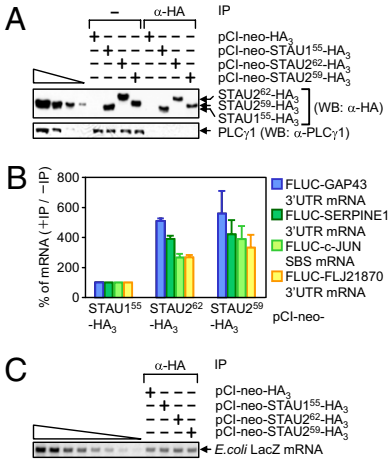

Fig. 4. $STAU2^{62}$-HA_3 and $STAU2^{59}$-HA_3 coimmunoprecipitate with known SBS-containing targets more efficiently than does $STAU1^{55}$-HA_3. HeLa cells (3×10^7 per 150-mm dish) were transiently transfected with 2 μg of each pcFLUC SMD-reporter plasmid, and 5 μg of pCI-neo-HA_3, pCI-neo-$STAU1^{55}$-HA_3, pCI-neo-$STAU2^{62}$-HA_3, or pCI-neo-$STAU2^{59}$-HA_3 effector plasmid. Two days later, lysates from formaldehyde-treated cells were immunoprecipitated using anti-HA, and cross-links were reversed. (*A*) WB of cell lysates after IP relative to before (–) IP using the specified antibody (α). PLCγ1 controlled for variations in protein loading before IP and demonstrates the specificity of the IP. The four left-most lanes show threefold dilutions of lysates from cells that expressed $STAU2^{59}$-HA_3. (*B*) RT-qPCR of FLUC mRNAs. For samples before IP, the level of each FLUC mRNA was normalized to the level of GAPDH mRNA, and the normalized level of FLUC mRNA from cells that expressed $STAU1^{55}$-HA_3 was defined as 100. For samples after IP, the level of each immunoprecipitated FLUC mRNA was normalized to its normalized level before IP. (*C*) After IP, samples were spiked with a small amount of *E. coli* RNA, and RT-PCR measurements of the level of *E. coli* LacZ mRNA confirmed comparable RNA recovery efficiencies.

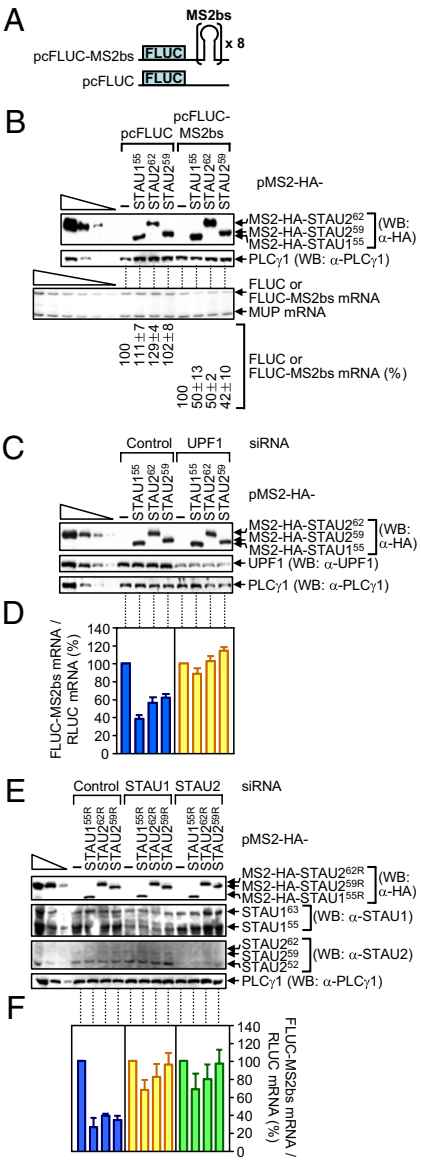

Fig. 5. Evidence that tethering MS2-HA-$STAU1^{55}$, MS2-HA-$STAU2^{62}$, or MS2-HA-$STAU2^{59}$ to the FLUC-MS2bs mRNA 3′ UTR triggers FLUC-MS2bs mRNA SMD in a mechanism that depends on the cellular STAU paralogs and cellular UPF1. (*A*) Schematic representations of pcFLUC and pcFLUC-MS2bs, where × 8 specifies eight tandem repeats of the MS2 coat protein-binding site (MS2bs). (*B*) HeLa cells (2.5×10^5 per well of a six-well plate) were cotransfected with 0.2 μg of pcFLUC or pcFLUC-MS2bs, 0.1 μg of phCMV-MUP, and 1 μg of the specified pMS2-HA-STAU effector plasmid. Two days after transfection, protein and RNA were purified. WB using anti(α)-HA demonstrated comparable levels of effector protein expression. (*B, Lower*) Using RT-PCR, normalized levels of FLUC or FLUC-MS2bs mRNA in the presence of the specified effector protein were calculated as a percentage of the normalized level of FLUC or FLUC-MS2bs mRNA in the presence of pMS2-HA, which was defined as 100. (*C* and *D*) HeLa cells (2.5×10^5 per well) were transiently transfected with 0.1 μg of pcFLUC-MS2bs, 0.1 μg of a plasmid that produces RLUC protein (pRLUC), which encodes renilla luciferase, and 1 μg of the specified effector plasmid. One day later, cells were transfected with specified siRNA. After an additional 2 d, protein and RNA were purified. (*C*) WB was used to quantitate the extent of down-regulation. (*D*) RT-qPCR was used to quantitate the effects of tethering of the specified protein on FLUC-MS2bs mRNA abundance. (*E* and *F*) Essentially as in *C* and *D*, except the effector plasmids were siRNA resistant (^{R}).

transfected with (*i*) a pcFLUC-MS2bs reporter construct that carries eight copies of the MS2 coat-protein binding sequence (MS2bs) in its 3′ UTR (13), or, as a negative control, pcFLUC

(Fig. 5*A*), (*ii*) phCMV-MUP, and (*iii*) pMS2-HA-STAU1^{55} (13), pMS2-HA-STAU2^{62}, or pMS2-HA-STAU2^{59}, each of which encodes a tetherable protein.

The expression of each tetherable protein reduced the abundance of FLUC-MS2bs reporter mRNA but not control FLUC mRNA to ~40–50% of normal (Fig. 5*B*). Using cells that were also transfected with Control or UPF1 siRNA (Fig. 5*C*), tethering not only STAU1^{55} (13, 14) but also STAU2^{62} or STAU2^{59} down-regulated FLUC-MS2bs reporter mRNA abundance to ~40–60% of normal, and down-regulating UPF1 inhibited this down-regulation (Fig. 5 *C* and *D*). Thus, tethered STAU2, like tethered STAU1, triggers SMD via its interaction with UPF1. Using cells transfected with Control, STAU1, or STAU2 siRNA (Fig. 5*E*), tethering STAU1^{55R}, STAU2^{62R}, or STAU2^{59R}, each of which was produced from an siRNA-resistant vector, again reduced FLUC-MS2bs reporter mRNA abundance to ~20–40% of normal (Fig. 5*F*). STAU1 siRNA inhibited the ability of tethered STAU1^{55R}, STAU2^{62R}, or STAU2^{59R} to reduce mRNA abundance, as did STAU2 siRNA (Fig. 5*F*). Thus, neither STAU2 nor STAU1 can efficiently trigger SMD when the level of cellular STAU2, STAU1, or UPF1 is reduced, indicating that both paralogs contribute to SMD via their interaction with each other and UPF1.

SMD Requires ATP-Dependent UPF1 Helicase Activity, Which Is Enhanced by STAU2 and STAU1 Without a Concomitant Enhancement of UPF1 ATPase Activity. Binding of the UPF2 NMD factor to the UPF1 CH domain promotes UPF1 ATPase and helicase activities in a way that is important for NMD (27, 28). Considering that STAU1 and STAU2 bind to a region of UPF1 that contains the CH domain (15, 16), we tested the importance of UPF1 ATPase and helicase activities to SMD by assaying UPF1 (G495R,G497E) (29), which fails to bind ATP (30, 31). Human UPF1 and UPF1(G495R,G497E) were produced in and purified from *E. coli* (Fig. S3*A*). ATPase activity assays were performed in the presence of γ-[^{32}P]ATP and, because the ATPase activity of UPF1 depends on RNA, poly(U) (30). The substrate for the helicase assays consisted of a 44-nt ssRNA annealed to an 18-nt γ-[^{32}P]-labeled ssDNA (28) (Fig. S3*C*), and assays were performed in the presence of excess unlabeled 18-nt ssDNA. In contrast to UPF1, UPF1(G495R,G497E) lacks both ATPase (Fig. 6*A*) and helicase (Fig. 6 *B* and *C*) activities.

Next, HEK293T cells were transiently transfected with a MYC-UPF1 or MYC-UPF1(G495R,G497E) expression vector (29) and a subset of the pcFLUC SMD-reporter plasmids (Fig. 1*B*). MYC-UPF1 proteins were each produced at a comparable level (Fig. 6*D*). Relative to MYC-UPF1, MYC-UPF1(G495R, G497E) inhibited SMD ~two- to fourfold (Fig. 6*E*). Thus, UPF1 binding to ATP and the resulting ATPase and/or helicase activities are important for SMD because of roles in SMD-target remodeling and/or indirectly because of roles in UPF1 recycling.

To characterize the dependence of UPF1 helicase activity on ATP hydrolysis, helicase assays were performed in the presence of ATP; 5′-adenylyl β,γ-imidodiphosphate (ADPNP), which is a nonhydrolyzable analog of ATP; ADP-BeF_3^-, which mimics the ground state of the ATP hydrolysis reaction (32); ADP-VO_3^-, which mimics the ADP+P_i transition state of ATP hydrolysis (33, 34); ATP together with $NaVO_3$, where VO_3^- replaces P_i after ATP hydrolysis to form ADP-VO_3^- at the active site and inhibit further hydrolysis (35–37); ADP; or no nucleotide. UPF1 helicase activity was evident in the presence of ATP and, to a lesser extent, in the presence of ATP+$NaVO_3$ but not in the absence of ATP or the presence of ADPNP, ADP-BeF_3^-, ADP-VO_3^-, or ADP (Fig. 6*F* and Fig. S3*D*). Thus, limiting ATP hydrolysis using ATP+$NaVO_3$ limits UPF1 helicase activity, and helicase activity is driven by the energy released from ATP cleavage and/or a resulting cleavage-dependent change in UPF1 conformation that is not recapitulated by any of the tested nucleotide analogs.

To determine the effect of STAU1 and STAU2 on UPF1 ATPase and helicase activities, the assays were repeated in the presence of increasing amounts of HIS-STAU1^{55}, STAU2^{62}, STAU2^{59}-HIS or, as a negative control, PABPC1. In the presence of poly(U) (Fig. 6*G*) or the RNA–DNA duplex (Fig. S3*E*), none of the STAU1 or STAU2 isoforms or PABPC1 manifested appreciable ATPase activity itself or enhanced UPF1 ATPase activity. However, in the presence of ATP all STAU isoforms, unlike PABPC1, activated UPF1 helicase activity in a concentration-dependent manner more or less to the same extent (Fig. 6*H* and Fig. S3*F*; we consider the low level of helicase activity manifested by HIS-STAU1^{55}, STAU2^{62}, STAU2^{59}-HIS, or PABPC1 alone to be background activity). STAU1 or STAU2 did not enhance UPF1 helicase activity in the absence of ATP (Fig. 6 *I* and *J* and Fig. S3 *G* and *H*) and also failed to activate UPF1 (G495R,G497E) helicase activity (Fig. 6*K*).

Results from our ATPase assays demonstrating that the STAU paralog-mediated enhancement of UPF1 unwinding is not accompanied by an increase in the number of ATP hydrolytic events predicts that limiting ATP hydrolysis using $NaVO_3$ to "trap" UPF1 in a state that inhibits further hydrolysis would not inhibit the effect of STAU1^{55} on UPF1 unwinding. In fact, when present in excess of ATP, $NaVO_3$ does not inhibit the ability of STAU1^{55}, STAU2^{62} and STAU2^{59} to augment UPF1 helicase activity (Fig. 6 *L* and *M* and Fig. S3 *I*–*L*). We propose that when UPF1 is bound by ATP or a specific catalytic intermediate of ATP hydrolysis—one that is not recapitulated by any of the nucleotide analogs tested here—STAU1, and possibly STAU2, promotes UPF1 helicase activity by inducing and/or stabilizing a helicase-active conformation.

Evidence That STAU2 Induces a Conformational Change in RNA-Bound UPF1. UPF2 augments UPF1 ATPase and helicase activities during NMD by binding to the UPF1 CH domain and, according to RNase protection assays, decreasing the UPF1 footprint on ssRNA (27). The decreased footprint was interpreted as a change in UPF1 conformation that loosened its grip on ssRNA, allowing it to unwind RNA more effectively.

We performed comparable RNA footprint experiments to determine whether STAU2^{62} changes UPF1 conformation. We examined STAU2^{62} because of its higher binding in vitro to UPF1 relative to STAU1^{55} or STAU2^{59} (Fig. 2*B*) and its greater solubility over STAU1^{55} under footprinting conditions. STAU2^{62} binding to UPF1 shifts the length of RNA protected by UPF1 from 11 to 12 nt to 12 to 13 nt (Fig. 7*A*, compare lanes 2 and 3), whereas in the absence of STAU2^{62}, ADPNP, ADP-AlF_4^-, or ADP-VO_3^- binding to UPF1 increased the length of RNA protected to 12–14 nt (Fig. 7*A*, compare lanes 5–7), and ADP binding further increased the length to 12–15 nt (Fig. 7*A*, lane 9). We propose that STAU2^{62} alters the conformation of UPF1 so that it protects a length of RNA that is between the length protected by ATP-free UPF1 and ATP (or an ATP-hydrolysis intermediate)-bound UPF1. Thus, STAU2^{62} binding enables UPF1 to approximate a conformation that is active in translocation and/or unwinding. In the absence of STAU2^{62}, the UPF1 footprint was not well defined when ATP or ATP+$NaVO_3$ was present (Fig. 7*A*, lanes 4 and 8) as expected because either UPF1 fails to bind RNA efficiently or the position of UPF1 on RNA is not fixed (Fig. 6 *F* and *M*). Although not proven, we do not believe that the increased footprint observed when STAU2^{62} is added to UPF1 is due to STAU2^{62} binding to ssRNA because STAU2^{62}, unlike STAU1^{55} (2), does not appreciably bind our RNA–DNA duplex (Fig. S4 *A* and *B*), which contains 26 nt of ssRNA. Moreover, STAU2 does not noticeably affect the ssRNA-binding activity of UPF1 (Fig. S4*B*). The simplest interpretation of our results is that the STAU2^{62}-mediated increase in UPF1 helicase activity is accompanied by an alteration in UPF1 conformation (Fig. 7 *B*–*D*).

Discussion

STAU2 Functions in SMD. Our results reveal that STAU2, like STAU1 (13), interacts directly with UPF1 both in vivo and in vitro, and these interactions are necessary for efficient SMD (Figs. 1, 2, and 5). Recently, Miki et al. (15) also demonstrated that STAU2 isoforms interact directly with UPF1 in vitro. In

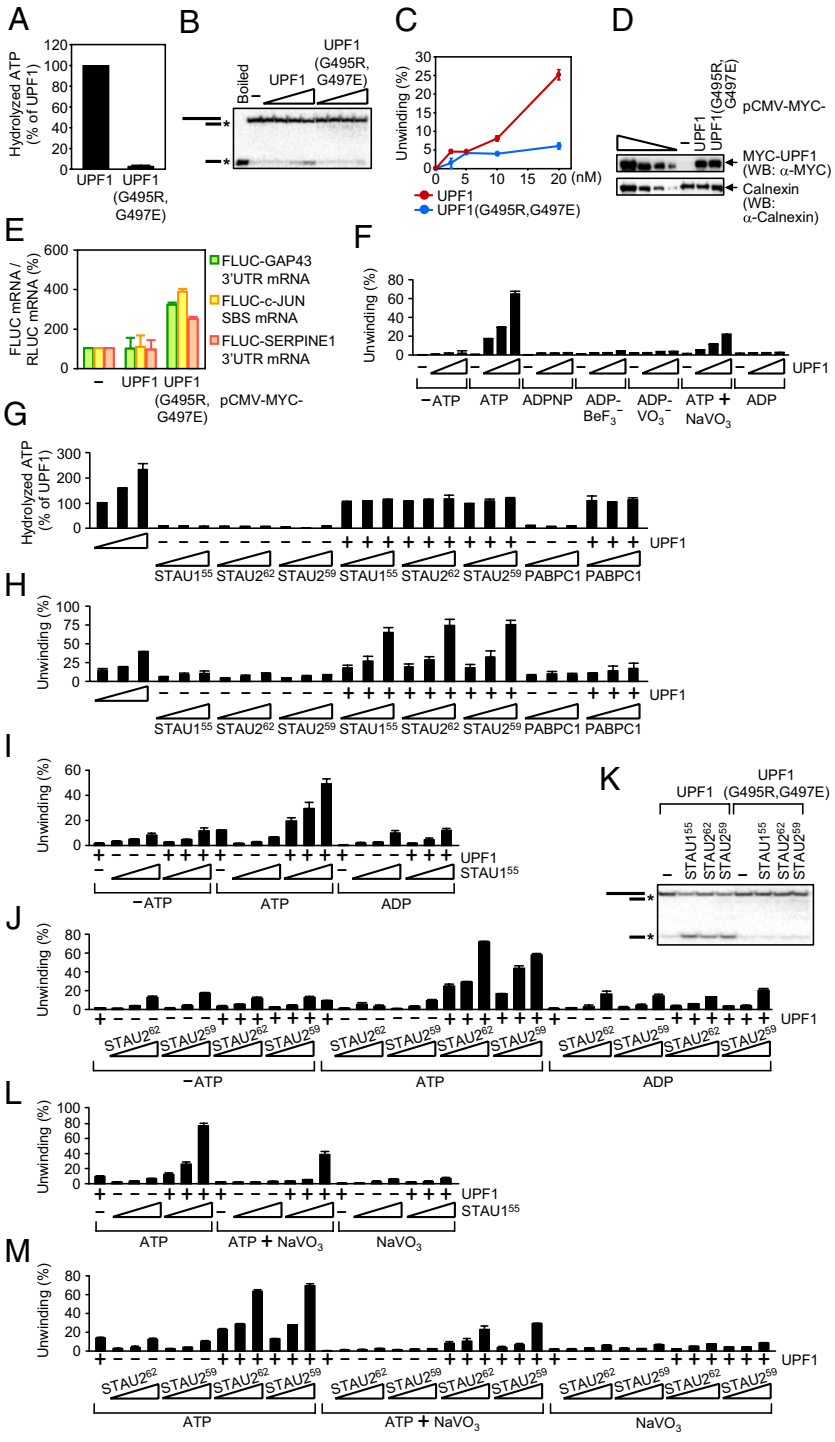

Fig. 6. STAU1[55], STAU2[62], and STAU2[59] activate SMD by augmenting UPF1 helicase activity but not UPF1 ATPase activity. (*A*) Histogram of RNA-dependent ATPase assays using 10 nM of UPF1 or UPF1(G495R, G497E), where the activity of UPF1 was defined as 100. Assays used 1 μCi of γ-[^{32}P]ATP and 4 μg of poly(U). (*B*) ATP-dependent helicase assays using 0 (–), 2.5, 5, 10, or 20 nM (wedge) of UPF1 or UPF1(G495R,G497E) in the presence of 0.25 nM of γ-[^{32}P]-labeled RNA–DNA duplex. Mobilities of the RNA–DNA duplex and ssDNA are indicated by cartoons, where the asterisk (*) denotes γ-[^{32}P]. (*C*) Plot of data in *B*. (*D* and *E*) HEK293T cells (4×10^7 per 150-mm dish) were transiently transfected with 1 μg of each pcFLUC SMD-reporter plasmid; 0.5 μg of the pRLUC reference plasmid; and 1 μg of pCMV-MYC(–), pCMV-MYC-UPF1, or pCMV-MYC-UPF1(G495R,G497E). Two days later, protein and RNA were purified. (*D*) WB using the specified antibody (α). The four left-most lanes show threefold dilutions of lysates from cells that expressed MYC-UPF1. (*E*) Histogram of RT-qPCR results. The level of each FLUC mRNA was normalized to the level of RLUC mRNA, and the normalized level of each in pCMV-MYC-transfected cells was defined as 100. (*F*) As in *B*, using 0 (–), 10, 20, or 40 nM (wedge) of UPF1 in the absence of nucleotide (–ATP) or in the presence of 0.5 mM of ATP, ADPNP, ADP-BeF_3^-, ADP-VO_3^-, or ADP, or 0.5 mM of ATP together with (+) 2.5 mM of $NaVO_3$ (Fig. S3*D*). (*G*) As in *A*, using 0 (–), 10, 20, or 40 nM of UPF1 (wedge) or 10 nM UPF1 (+) and/or 10, 20, or 40 nM of HIS-STAU1[55], STAU2[62], STAU2[59]-HIS, or PABPC1 (wedge). (*H*) Helicase assays (Fig. S3*F*) using samples assayed in *G*. (*I* and *J*) As in *B*, using 0 (–) or 10 nM of UPF1 (+) and/or 10, 20, or 40 nM (wedge) of (*I*) HIS-STAU1[55], (*J*) STAU2[62] or STAU2[59]-HIS in the absence of nucleotide (–ATP) or in the presence of 2 mM of ATP or ADP (Fig. S3 *G* and *H*). (*K*) As in *B*, using 10 nM of UPF1 or UPF1(G495R,G497E) and 0 (–) or 40 nM of HIS-STAU1[55], STAU2[62], or STAU2[59]-HIS. (*L* and *M*) Helicase assays (Fig. S3 *K* and *L*) as in *I* and *J*, in the presence of 2 mM of ATP, 2 mM of ATP+10 mM of $NaVO_3$, or 10 mM of $NaVO_3$.

support of STAU2 function during SMD, tethering STAU2 downstream of the termination codon of a reporter mRNA, like tethering STAU1, reduces reporter mRNA abundance in HEK293T cells in a mechanism that depends on UPF1, STAU1, and STAU2 (Fig. 5). Additionally, the efficiency of SMD in tethering assays and assays of cellular targets is determined by the abundance of both STAU1 and STAU2 (Fig. 5, Fig. S5, and *SI Discussion*). Our finding that the two STAU paralogs interact directly suggests that any functional differences between the two paralogs during SMD would be homogenized, but less so for tissues in which one paralog is significantly more abundant than the other.

STAU2–STAU2, STAU2–STAU1, and STAU1–STAU1 interactions are readily detected (Fig. 3) and may be required for optimal UPF1 binding and/or activation. For example, our finding that STAU1 stabilizes imperfect intermolecular RNA duplexes that range in size from ~85 to 300 bp (17) suggests that STAU association contributes to duplex stabilization. Unlike Furic et al. (20), we find no evidence for STAU1- or STAU2-specific mRNA targets (Fig. 4). Given that the paralogs interact, it is difficult to conceive of such targets unless there were conditions whereby one paralog is significantly more abundant than the other.

STAU1–STAU1 interactions have been shown using live cells to involve dsRBD2 and dsRBD5 (22). Because STAU1

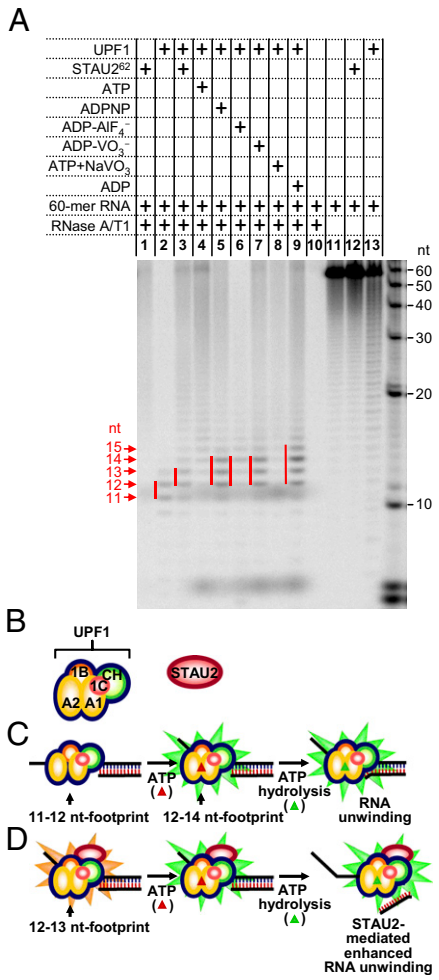

Fig. 7. STAU2^{62} expands the UPF1 footprint on ssRNA. (*A*) The specified complexes were formed using 5 pmol of in vitro-transcribed α-[^{32}P]UTP-labeled 60-nt RNA; 10 pmol of UPF1; 40 pmol of STAU2^{62}; and where specified 2 mM of the indicated nucleotide and 10 mM of the specified phosphate mimic. Notably, ADP-BeF_3^- was not tested because a precipitate formed at 10 mM BeF_3^-. Samples were then incubated with 1 μg of RNase A and 1 U of RNase T1. The sizes of the protected RNA fragments were determined using denaturing polyacrylamide gel electrophoresis followed by autoradiography. A γ-[^{32}P]-labeled RNA ladder provided molecular weight standards (black nt), and red notations denote protected fragments. Notably, sizes assigned to the protected fragments were confirmed in gels, in which molecular weight standards were eletrophoresed in lanes residing adjacent to each experimental lane. The nature of the diffuse ∼6-nt band that was evident in the presence of all tested nucleotides requires further investigation. The footprint in the presence of ADP-AlF_4^- was routinely faint. (*B–D*) Model for how STAU paralogs bind to and prolong a conformational state of UPF1 that promotes its ATP-dependent unwinding activity without promoting ATP hydrolysis. (*B*) Domains of UPF1, where A1 and A2 represent the two RecA-like domains, 1B is an N-terminal attachment of the A1 domain, 1C is an insertion in the A1 domain, and CH denotes the cysteine- and histidine-rich region (27, 31). (*C*) ATP-free UPF1 protects a smaller (11- to 12-nt) region of RNA than does ATP-bound UPF1. The footprint of ATP-bound UPF1 consists of as many as 14 nt and is maintained during the process of ATP hydrolysis and RNA unwinding. Additional rounds of ATP hydrolysis lead to more extensive duplex unwinding. (*D*) STAU2 association with UPF1 generates the larger UPF1 footprint that typifies UPF1 bound to ATP or a hydrolytic intermediate (e.g., ADPNP, ADP-VO_3^-, or ADP). Because STAU2 does not bind ssRNA, we infer that STAU2 alters the conformation of ssRNA-bound UPF1 (surrounding yellow spikes) so UPF1 is better poised to receive ATP and/or unwind RNA when ATP is already bound (surrounding green spikes). In this way, STAU2 enhances the intrinsic unwinding capability of UPF1 per ATP hydrolyzed. UPF1 helicase activity has been shown to scan and remodel mRNP during NMD (45, 46).

dsRBD2 and parts of STAU1 dsRBD5 are conserved in all STAU2 isoforms (Fig. 1), it is possible that STAU1–STAU2 and STAU2–STAU2 interactions are also mediated by dsRBD2 and dsRBD5. Relative to STAU1, the binding of STAU2 to SBS-containing mRNAs is ∼two- to fivefold higher (Fig. 4), which might be due to the additional dsRBD, dsRBD1, in STAU2 compared with STAU1 (Fig. 1). However, because dsRBD3 and dsRBD4 seem to be the only functional dsRNA-binding domains (1, 2), contributions to RNA binding by dsRBD1 or by other differences between STAU2 and STAU1 might enhance STAU2 dsRBD3 and/or dsRBD4 function. For example, individual dsRBDs that do not bind dsRNA in vitro can promote dsRNA binding of a "true" dsRBD when both reside in tandem as exemplified by *Xenopus laevis* RNA-binding protein A (38).

Deletion analyses indicate that STAU1 (16) and STAU2 (15) interact with a region of UPF1 that includes the CH domain. This is the same region of UPF1 that interacts with UPF2 during NMD. Relative to STAU1, the binding of STAU2 to UPF1 is ∼10-fold higher (Fig. 2). Considering that residues spanning the TBD to just upstream of dsRBD5 seem to be the minimal region of STAU1 that interacts with UPF1 (16), differences in the binding of STAU2 and STAU1 to UPF1 may be attributable to sequence variations in their TBDs, which share only 18% identity (Fig. 1). Provided the paralogs bind tightly enough to overcome the activation threshold for UPF1 helicase activity, they may bind to overlapping or different regions of the CH domain with different efficiencies yet still activate UPF1 helicase activity to the same extent (Fig. 6). Alternatively, STAU2 may interact with UPF1 using an entirely different region, such as dsRBD2 or dsRBD3 (15).

STAU2 Stimulates UPF1 Unwinding Activity but Not UPF1 ATP Hydrolytic Activity and Induces a Conformational Change in UPF1. When added to UPF1, higher concentrations of STAU2 or STAU1 increase higher levels of UPF1 RNA–DNA duplex unwinding without stimulating UPF1 ATPase activity in a mechanism that depends on the presence and/or hydrolysis of ATP (Fig. 6). There are two key differences between how STAU2 and STAU1 activate UPF1 during SMD and how UPF2 activates UPF1 during NMD (27). First, UPF2 stimulates UPF1 ATPase activity, whereas the STAU paralogs do not; they merely "grease the wheels" of the UPF1 helicase so that unwinding is more extensive per ATP hydrolyzed. Second, at least for STAU2^{62}, activation of UPF1 helicase activity is achieved by increasing rather than decreasing the UPF1 footprint on RNA (Fig. 7). It has been reported that UPF2 in the presence of ADP-BeF_3 decreases the size of the UPF1 footprint (27), UPF2 in the absence of nucleotide analog loosens the grip of UPF1 on RNA (28), and UPF2 in the presence of ATP enhances UPF1 helicase activity (27). Although at pH 6.5 the footprint of UPF1 alone (28) was found to be similar in size to the footprint of UPF1 in the presence of ADPNP (27, 28), we are able to detect a difference in the size of the two footprints at the more physiological pH 7. We report here that UPF1 alone, which has a higher affinity for ssRNA than when nucleotide bound (27, 31), has a smaller footprint than when nucleotide bound. Therefore, the correlation of a smaller UPF1 footprint with activation of UPF1 helicase activity, as observed in studies using UPF2 (27), may not be universal, as evidenced from our studies using STAU2, which indicate that a larger UPF1 footprint correlates with activation of UPF1 helicase activity. Because nucleotide binding lowers the association of UPF1 with RNA (27, 31), and a lowered association correlates with enhanced helicase activity (27), STAU2^{62} binding to UPF1 may mimic nucleotide binding. UPF1 may resemble the human coronavirus 229E helicase, which is capable of unwinding long stretches of duplexed RNA before dissociating (39), except that the processivity of UPF1 is augmented by its binding to one or both STAU cofactors.

There are other examples of cofactor-mediated helicase activation that seem to bypass coordinated ATPase stimulation. Ntr1 of the Ntr1/Ntr2 complex enhances Prp43 RNA helicase activity

in an ATP-dependent manner but without an apparent enhancement of ATPase activity (40, 41). As a variation of this theme, the *E. coli* Rep DNA helicase uses ATP hydrolysis not for unwinding but for translocation to a dsDNA structure and, by analogy to how STAU cofactors activate the UPF1 helicase, the ØX174 gene A protein or constituents of the multi-Rep complex then promote *E. coli* Rep helicase activity (42, 43). Taking cues from these and other studies, we propose that STAU2 and possibly STAU1 stabilize UPF1 in a conformation that is active during unwinding and/or translocation (Fig. 7).

Summary. We envision that STAU1 and/or STAU2 bind to an SBS either individually or, more likely, as homo- or heteromultimers, the size of which may depend on the length of the SBS and the relative abundance of each paralog. STAU bound to an SBS recruits UPF1 either directly or through interactions with another STAU molecule, presumably after translation terminates if a comparison can be made to when UPF1 binds the stem-loop binding protein of cell cycle-regulated histone mRNAs (44). By analogy to the mechanism of NMD, after translation terminates sufficiently upstream of the SBS, STAU–UPF1 then reconfigures so that the helicase activity of UPF1 is activated by STAU.

Materials and Methods

Descriptions of plasmid constructions; cell transfection and lysis, and cell protein and RNA purification are given in *SI Materials and Methods*. *Supporting Information* also provides details for recombinant protein purification and in vitro pull-down experiments. See *SI Materials and Methods* for in vitro ATPase and helicase assays; and RNase protection assays.

ACKNOWLEDGMENTS. We thank Susana de Lucas and Juan Ortín for anti-STAU1, David Bear for the GST-PABPC1 plasmid, Yalan Tang for baculovirus-produced FLAG-UPF1, Galina Pavlencheva for *E. coli*-produced UPF1 and UPF1 (G495R,G497E), and Dmitri Ermolenko, Joseph Wedekind, Eckhard Jankowsky, Hérve Le Hir, Fabien Bonneau, and L.E.M. laboratory members for advice. This work was funded by National Institutes of Health (NIH) Grant R01 GM074593 (to L.E.M.). E.P. was supported by American Heart Association Founders Affiliate Postdoctoral Fellowship 11POST 7860051. M.L.G. was supported by NIH Grant F32 GM090479 and NIH National Cancer Institute Grant T32 CA09363.

1. Duchaîne TF, et al. (2002) Staufen2 isoforms localize to the somatodendritic domain of neurons and interact with different organelles. *J Cell Sci* 115(Pt 16):3285–3295.
2. Wickham L, Duchaîne T, Luo M, Nabi IR, DesGroseillers L (1999) Mammalian staufen is a double-stranded-RNA- and tubulin-binding protein which localizes to the rough endoplasmic reticulum. *Mol Cell Biol* 19(3):2220–2230.
3. Monshausen M, Gehring NH, Kosik KS (2004) The mammalian RNA-binding protein Staufen2 links nuclear and cytoplasmic RNA processing pathways in neurons. *Neuromolecular Med* 6(2-3):127–144.
4. Kanai Y, Dohmae N, Hirokawa N (2004) Kinesin transports RNA: Isolation and characterization of an RNA-transporting granule. *Neuron* 43(4):513–525.
5. Kiebler MA, et al. (1999) The mammalian staufen protein localizes to the somatodendritic domain of cultured hippocampal neurons: Implications for its involvement in mRNA transport. *J Neurosci* 19(1):288–297.
6. Thomas MG, et al. (2005) Staufen recruitment into stress granules does not affect early mRNA transport in oligodendrocytes. *Mol Biol Cell* 16(1):405–420.
7. Vessey JP, et al. (2008) A loss of function allele for murine Staufen1 leads to impairment of dendritic Staufen1-RNP delivery and dendritic spine morphogenesis. *Proc Natl Acad Sci USA* 105(42):16374–16379.
8. Tang SJ, Meulemans D, Vazquez L, Colaco N, Schuman E (2001) A role for a rat homolog of staufen in the transport of RNA to neuronal dendrites. *Neuron* 32(3): 463–475.
9. Goetze B, et al. (2006) The brain-specific double-stranded RNA-binding protein Staufen2 is required for dendritic spine morphogenesis. *J Cell Biol* 172(2):221–231.
10. Lebeau G, et al. (2008) Staufen1 regulation of protein synthesis-dependent long-term potentiation and synaptic function in hippocampal pyramidal cells. *Mol Cell Biol* 28(9):2896–2907.
11. Lebeau G, DesGroseillers L, Sossin W, Lacaille JC (2011) mRNA binding protein staufen 1-dependent regulation of pyramidal cell spine morphology via NMDA receptor-mediated synaptic plasticity. *Mol Brain* 4:22.
12. Lebeau G, et al. (2011) Staufen 2 regulates mGluR long-term depression and Map1b mRNA distribution in hippocampal neurons. *Learn Mem* 18(5):314–326.
13. Kim YK, Furic L, DesGroseillers L, Maquat LE (2005) Mammalian Staufen1 recruits Upf1 to specific mRNA 3'UTRs so as to elicit mRNA decay. *Cell* 120(2):195–208.
14. Kim YK, et al. (2007) Staufen1 regulates diverse classes of mammalian transcripts. *EMBO J* 26(11):2670–2681.
15. Miki T, et al. (2011) Cell type-dependent gene regulation by Staufen2 in conjunction with Upf1. *BMC Mol Biol* 12:48.
16. Gong C, Kim YK, Woeller CF, Tang Y, Maquat LE (2009) SMD and NMD are competitive pathways that contribute to myogenesis: Effects on PAX3 and myogenin mRNAs. *Genes Dev* 23(1):54–66.
17. Gong C, Maquat LE (2011) lncRNAs transactivate STAU1-mediated mRNA decay by duplexing with 3′ UTRs via Alu elements. *Nature* 470(7333):284–288.
18. Cho H, et al. (2012) Staufen1-mediated mRNA decay functions in adipogenesis. *Mol Cell* 46(4):495–506.
19. Gautrey H, McConnell J, Lako M, Hall J, Hesketh J (2008) Staufen1 is expressed in preimplantation mouse embryos and is required for embryonic stem cell differentiation. *Biochim Biophys Acta* 1783(10):1935–1942.
20. Furic L, Maher-Laporte M, DesGroseillers L (2008) A genome-wide approach identifies distinct but overlapping subsets of cellular mRNAs associated with Staufen1- and Staufen2-containing ribonucleoprotein complexes. *RNA* 14(2):324–335.
21. Allison R, et al. (2004) Two distinct Staufen isoforms in *Xenopus* are vegetally localized during oogenesis. *RNA* 10(11):1751–1763.
22. Martel C, et al. (2010) Multimerization of Staufen1 in live cells. *RNA* 16(3):585–597.
23. Pal M, Ishigaki Y, Nagy E, Maquat LE (2001) Evidence that phosphorylation of human Upfl protein varies with intracellular location and is mediated by a wortmannin-sensitive and rapamycin-sensitive PI 3-kinase-related kinase signaling pathway. *RNA* 7(1):5–15.
24. Hwang J, Sato H, Tang Y, Matsuda D, Maquat LE (2010) UPF1 association with the cap-binding protein, CBP80, promotes nonsense-mediated mRNA decay at two distinct steps. *Mol Cell* 39(3):396–409.
25. Hosoda N, Kim YK, Lejeune F, Maquat LE (2005) CBP80 promotes interaction of Upf1 with Upf2 during nonsense-mediated mRNA decay in mammalian cells. *Nat Struct Mol Biol* 12(10):893–901.
26. Maher-Laporte M, et al. (2010) Molecular composition of staufen2-containing ribonucleoproteins in embryonic rat brain. *PLoS ONE* 5(6):e11350.
27. Chakrabarti S, et al. (2011) Molecular mechanisms for the RNA-dependent ATPase activity of Upf1 and its regulation by Upf2. *Mol Cell* 41(6):693–703.
28. Chamieh H, Ballut L, Bonneau F, Le Hir H (2008) NMD factors UPF2 and UPF3 bridge UPF1 to the exon junction complex and stimulate its RNA helicase activity. *Nat Struct Mol Biol* 15(1):85–93.
29. Isken O, Maquat LE (2008) The multiple lives of NMD factors: Balancing roles in gene and genome regulation. *Nat Rev Genet* 9(9):699–712.
30. Bhattacharya A, et al. (2000) Characterization of the biochemical properties of the human Upf1 gene product that is involved in nonsense-mediated mRNA decay. *RNA* 6(9):1226–1235.
31. Cheng Z, Muhlrad D, Lim MK, Parker R, Song H (2007) Structural and functional insights into the human Upf1 helicase core. *EMBO J* 26(1):253–264.
32. Gu M, Rice CM (2010) Three conformational snapshots of the hepatitis C virus NS3 helicase reveal a ratchet translocation mechanism. *Proc Natl Acad Sci USA* 107(2): 521–528.
33. Lindquist RN, Lynn JL, Jr., Lienhard GE (1973) Possible transition-state analogs for ribonuclease. The complexes of uridine with oxovanadium(IV) ion and vanadium(V) ion. *J Am Chem Soc* 95(26):8762–8768.
34. Westheimer FH (1987) Why nature chose phosphates. *Science* 235(4793):1173–1178.
35. Goodno CC (1979) Inhibition of myosin ATPase by vanadate ion. *Proc Natl Acad Sci USA* 76(6):2620–2624.
36. Goodno CC, Taylor EW (1982) Inhibition of actomyosin ATPase by vanadate. *Proc Natl Acad Sci USA* 79(1):21–25.
37. Yamasaki K, Yamamoto T (1991) Existence of high- and low-affinity vanadate-binding sites on Ca(2+)-ATPase of the sarcoplasmic reticulum. *J Biochem* 110(6):915–921.
38. Krovat BC, Jantsch MF (1996) Comparative mutational analysis of the double-stranded RNA binding domains of *Xenopus laevis* RNA-binding protein A. *J Biol Chem* 271(45):28112–28119.
39. Ivanov KA, Ziebuhr J (2004) Human coronavirus 229E nonstructural protein 13: Characterization of duplex-unwinding, nucleoside triphosphatase, and RNA 5′-triphosphatase activities. *J Virol* 78(14):7833–7838.
40. Tanaka N, Aronova A, Schwer B (2007) Ntr1 activates the Prp43 helicase to trigger release of lariat-intron from the spliceosome. *Genes Dev* 21(18):2312–2325.
41. Tsai RT, et al. (2005) Spliceosome disassembly catalyzed by Prp43 and its associated components Ntr1 and Ntr2. *Genes Dev* 19(24):2991–3003.
42. Ha T, et al. (2002) Initiation and re-initiation of DNA unwinding by the *Escherichia coli* Rep helicase. *Nature* 419(6907):638–641.
43. Yarranton GT, Gefter ML (1979) Enzyme-catalyzed DNA unwinding: studies on *Escherichia coli* rep protein. *Proc Natl Acad Sci USA* 76(4):1658–1662.
44. Kaygun H, Marzluff WF (2005) Regulated degradation of replication-dependent histone mRNAs requires both ATR and Upf1. *Nat Struct Mol Biol* 12(9):794–800.
45. Franks TM, Singh G, Lykke-Andersen J (2010) Upf1 ATPase-dependent mRNP disassembly is required for completion of nonsense- mediated mRNA decay. *Cell* 143(6): 938–950.
46. Shigeoka T, Kato S, Kawaichi M, Ishida Y (2012) Evidence that the Upf1-related molecular motor scans the 3′-UTR to ensure mRNA integrity. *Nucleic Acids Res* 40(14): 6887–6897.